Electronic Supplementary Material (ESI) for Journal of Materials Chemistry C.

Supporting Information

Ultrafast Formation of NiFe Electrocatalysts by Fenton-assisted Corrosion Strategy for Alkaline Water and Urea Oxidation

Jianan Li, [1,†] Wenbo Sun, [2,†], Meng Zhang, [3,*] Jiutao An ,[2] Peiling Gao [2] and Chong Peng [4,*]

1 National Engineering Research Center of Industrial Wastewater Detoxication and Resource Recovery, East China University of Science and Technology, Shanghai, 200237, China

2 School of Resources and Environmental Engineering, Shandong University of Technology, Zibo, 255000, China

3 Institute of Applied Ecology, Chinese Academy of Sciences, Shenyang, 110016, China

4 School of Sensing Science and Engineering, Shanghai Jiao Tong University, Shanghai, 200240, China

† These authors contributed equally to this work.

Corresponding authors: zhangmeng@ecust.edu.cn; pengchong@dlut.edu.cn;

1. EXPERMENTAL DETAILS

1.1 Reagents and Materials

All chemicals were purchased from Shanghai Aladdin Bio-Chem Technology Co., LTD and directly used without further purification. The solution employed in the whole experiment were prepared with deionized water (D.I. water) supplied by a Milli-Q machine. The nickel foams (thickness = 1.6 mm) were purchased from the Tanqi New Materials Technology Department, Shanghai.

1.2 Synthesis of NiFe Hydroxide Electrocatalysts

The NiFe hydroxide electrocatalysts were prepared by a facile strategy combining classic homogenous Fenton treatment and replacement reaction together. Briefly, the nickel foam was successively washed by acetone, ethanol, and water by the ultrasonic treatment for 5 min. Then, the clean nickel foam was immersed into 10 mL $FeCl_3$ solution (0.1 M) with a certain amount of H_2O_2 (~30 wt%) added to trigger the redox reaction between Ni metal and Fe^{3+}. The generated Fe^{3+} would induce the Fenton process to form oxidative species, synergistically etching the pristine nickel foam. After a certain time, the obtained electrode sample was taken out and washed by D.I. water for several times, which was named as F-NiFe LDH-NF. For comparison, the normal $FeCl_3$ etching method was also employed to prepared the NiFe LDH-NF catalysts.

1.3 Characterizations and Measurements

Scanning electron microscope (SEM) was conduct on the HITACHI S4800 to observe the micro-morphology. X-ray photoelectron spectroscopy (XPS) was conducted on a PHI 5000 Versa 31 Probe spectrometer with an X-ray source of Al Kα to characterize the chemical atmosphere and status before and after electrolysis reaction. Specially, the obtained results were calibrated by the C 1s binding energy at 284.6 eV. X-ray diffraction (XRD) was carried out on the Rigaku Corporation D/Max-2400 with Cu Kα radiation (λ = 0.15418 nm) at a scan rate of 5 °/min. Raman spectra was obtained by using the laser of 532 nm. The electrochemical measurement was put forwards in a classic three-electrode system, in which Hg/HgO and graphite rod were selected as the reference and counter electrode respectively. To eliminate the possible interference of oxidation current from Ni^{2+} to Ni^{3+}, a reverse scan of LSV curve is always adopted as previously reported[1-5]. All the potentials employed were converted referring to the reverse hydrogen electrode (RHE). Electrochemical impedance spectra (EIS) were recorded from 0.01 to 1000000 Hz at different applied potentials. Electrochemical specific areas were obtained by conducting cyclic voltage measurement in the non-Faradaic zone to obtain the double-layer capacitance (C_{dl})[6].

2. DISCUSSIONS

2.1 Electrochemical Characterizations

Electrochemical impedance spectroscopy (EIS) was also performed to study the interface structure and charge transfer process (Figure S3). These plots were simulated by an equivalent circuit of simple Randle mode, in which the interception with horizontal axis represents the resistance of the system (R_s), the semicircle diameter equivalents the interface charge-transfer resistance (R_{ct}), and the space-charge capacitance (C_{sc}) parallel to R_{ct}. Nyquist plots showed F-NiFe LDH-NF exhibited smaller R_{ct} at the interface compared with that in NF and NiFe LDH-NF under the bias potential beyond 1.47 V (vs. RHE). It proved the better interface structure and conditions for charge exchange. Additionally, the Bode phase plots consisted two electrochemical processes caused by the electrode-electrolyte interface (low-frequency region) and the electro-oxidation of the electrode (middle-frequency region)[7]. Thus, the phase angle peaks in the low-frequency zone could be associated with the OH^- adsorption, while the one in the high-frequency zone indicates the OER. From the results, Fe involved could facilitate the OH^- adsorption into OER under lower potentials[8]. Moreover, F-NiFe LDH-NF behaved a more advanced posture towards high-frequency zone, proving its superior OER activity. This evidence well proved the advantages of Fenton involved in the synthesis of efficient NiFe electrocatalysts.

2.2 Influence Factors of Fenton-assisted etching method

To optimize parameters, the effect of H_2O_2 amount and treatment time on the electrochemical activity were further investigated in detail (Figure S4). The electrochemical OER activity increased with H_2O_2 amount at the initial, while the OER activity would be inhibited once beyond 2 mL. This could be explained by the structure collapse with a strong etching in the process. Although the C_{dl} still increased with H_2O_2 amount, the difference between the electrodes obtained from 2 mL and 4 ml H_2O_2 addition was not obvious. Meanwhile, a better OER activity of F-NiFe LDH-NF was gradually achieved with a longer Fenton-assisted etching time and 15 min was enough to get an outstanding performance. It could be inferred by effectively promoting exposure of reactive sites and continuously reshaping the surface structures during longer treatment time. However, when extended the treatment time into half an hour, it showed that the OER performed a less activity compared with that in 15 min. The electrochemical dynamic mechanism nearly kept the same from Tafel plots. This phenomenon could be same to that in the effect of larger H_2O_2 amount that over-corrosion could break up the hierarchical structure and destroy the reactive sites exposed. Only suitable etching degree of treatment could achieve the effective surface modification and induce abundant reactive sites to improve the electrochemical activity. Thus, the optimized conditions of electrode synthesis were adopted in the follow-up experiments to obtain the best electrochemical activity (2 mL H_2O_2 and 15 min treatment). We also compared the electrochemical performance by over-potential (η) at 10 mA/cm^2 and Tafel slope with previous literature[9-16]. Our work is located at a favorable position, superior

to many transition-metal-based OER catalysts, indicating the excellent performance achieved by this novel synthesis strategy.

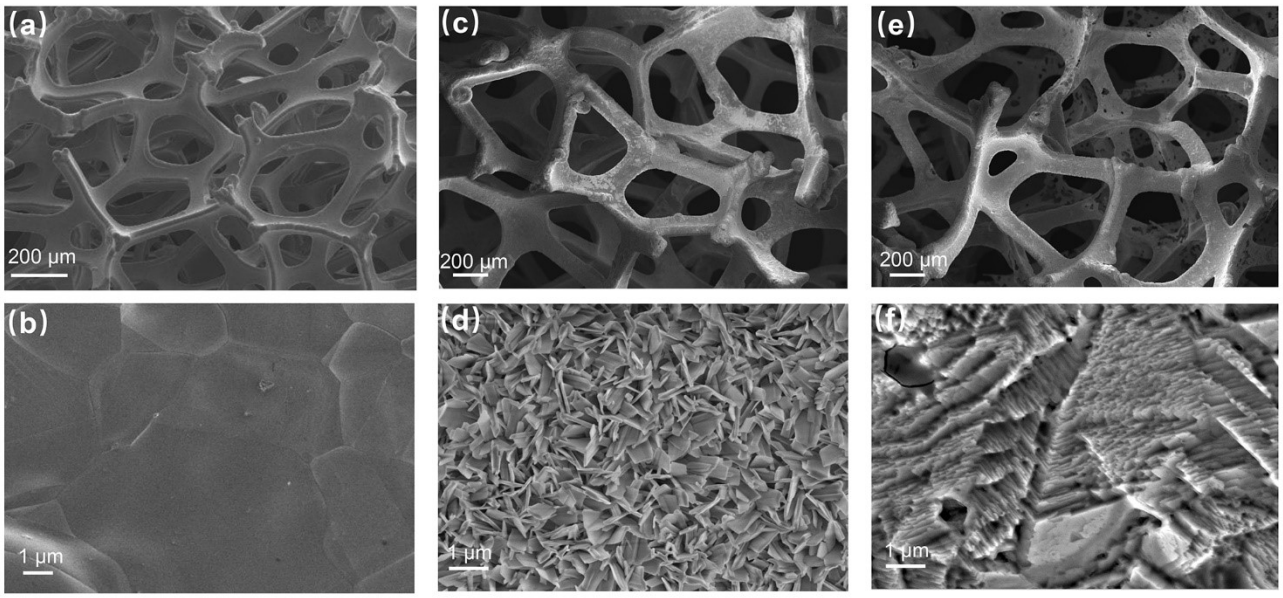

Figure S1 SEM images of (a, b) Ni foam, (c, d) NiFe LDH-NF electrode, and (e, f) F-NiFe LDH-NF electrode under different magnifications.

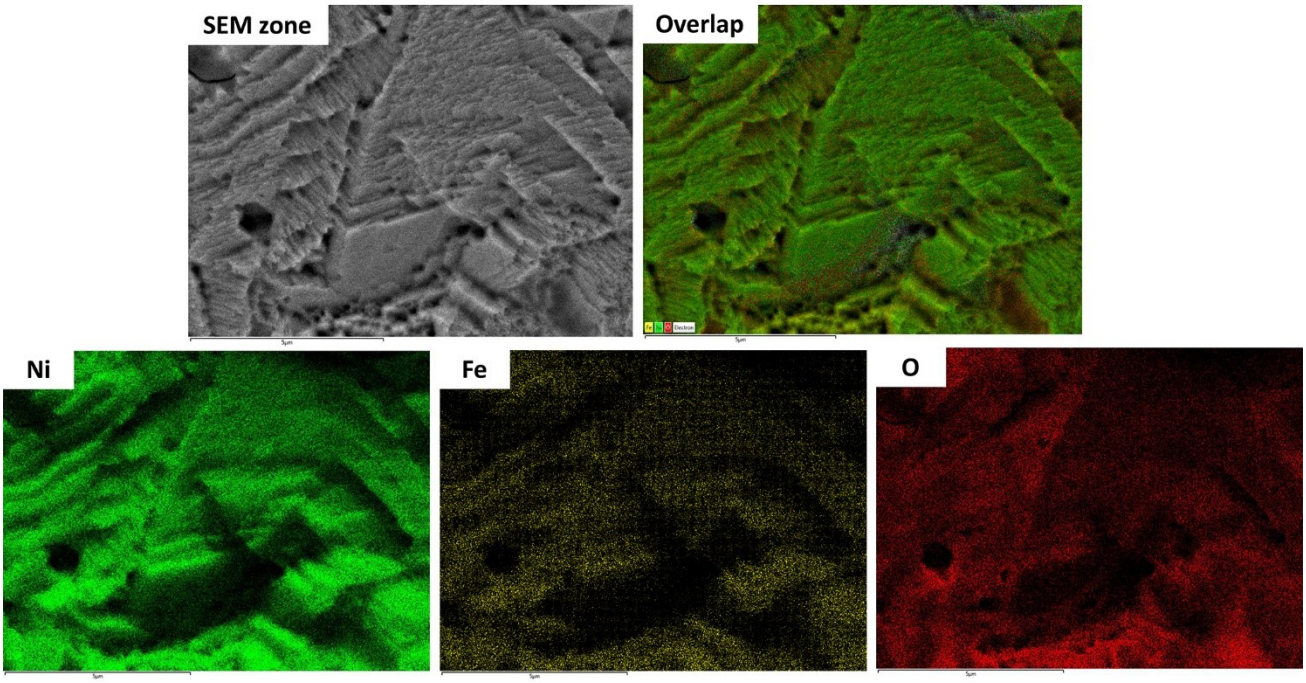

Figure S2 The energy dispersive spectrometer (EDS) analysis of elemental distribution on the F-NiFe LDH-NF electrode surface.

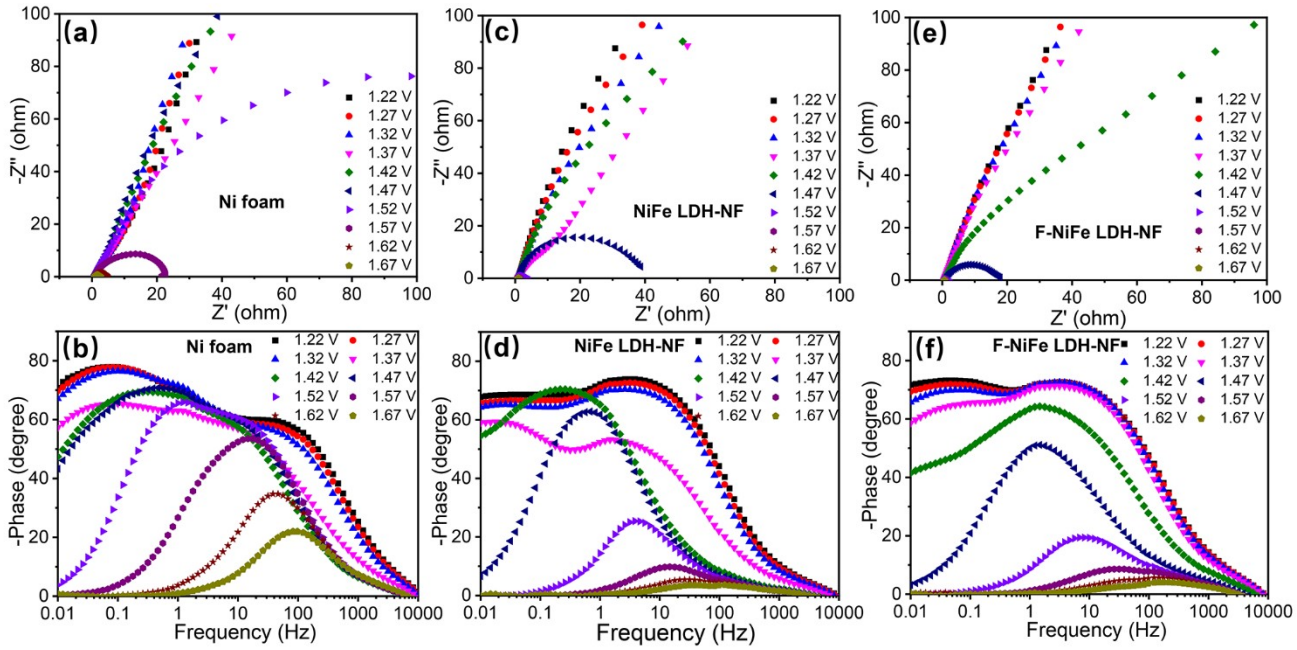

Figure S3 The Nyquist and Bode plots of (a, b) Ni foam, (c, d) NiFe LDH-NF, and (e, f) F-NiFe LDH-NF electrodes under a series of applied potentials respectively.

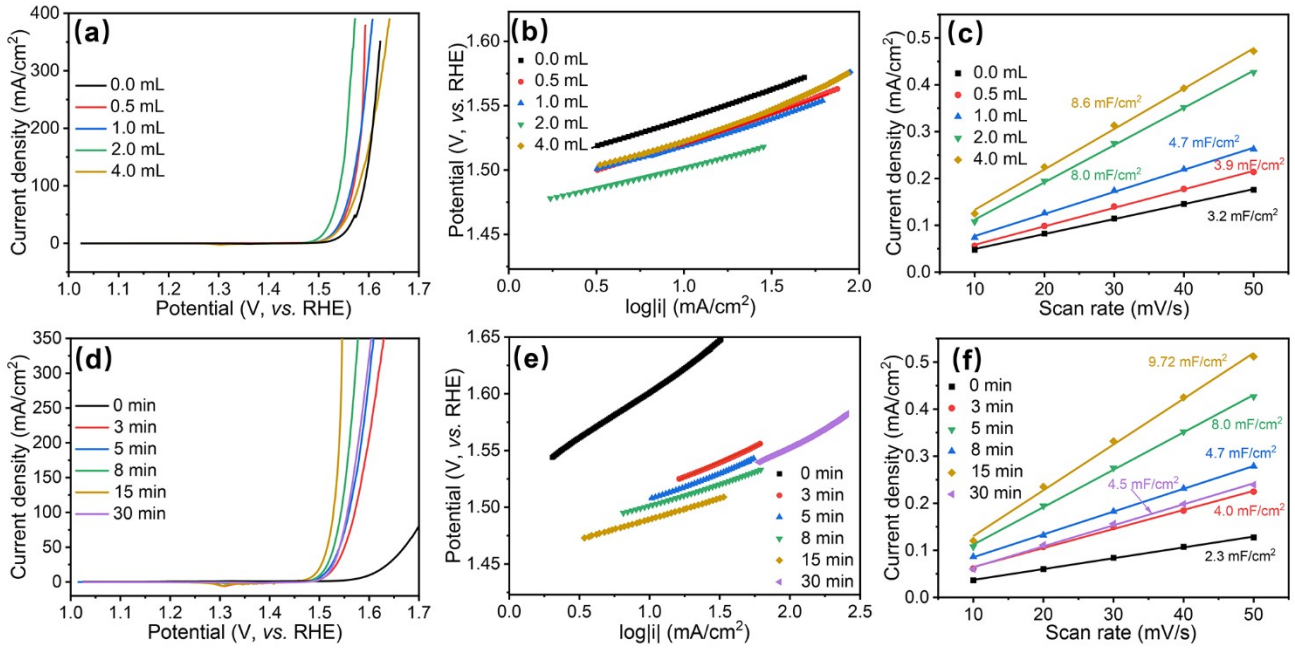

Figure S4 (a) Polarization curves, (b) Tafel plots, and (c) ECSA calculations of F-NiFe LDH-NF electrodes under different H_2O_2 addition. (d) Polarization curves, (e) Tafel plots, and (f) ECSA calculations of F-NiFe LDH-NF electrodes under different treatment time.

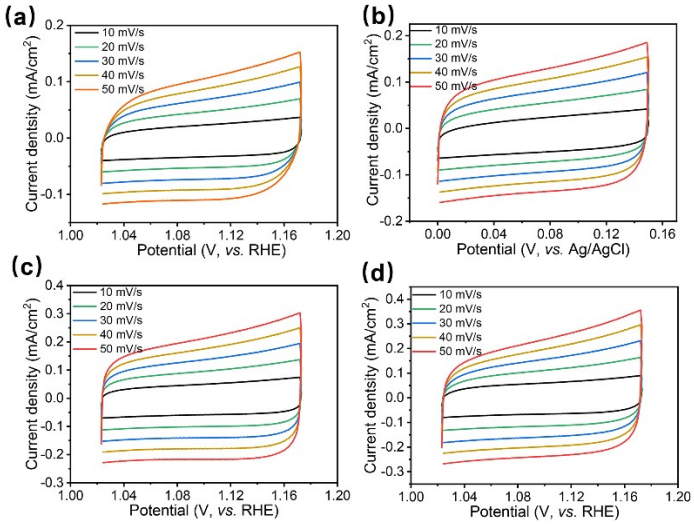

Figure S5 CV curves of F-NiFe LDH-NF electrodes at different scan rates from 10 to 50 mV/s with (a) 0.5 mL, (b) 1 mL, (c) 2 mL, and (d) 4 mL H_2O_2 addition respectively.

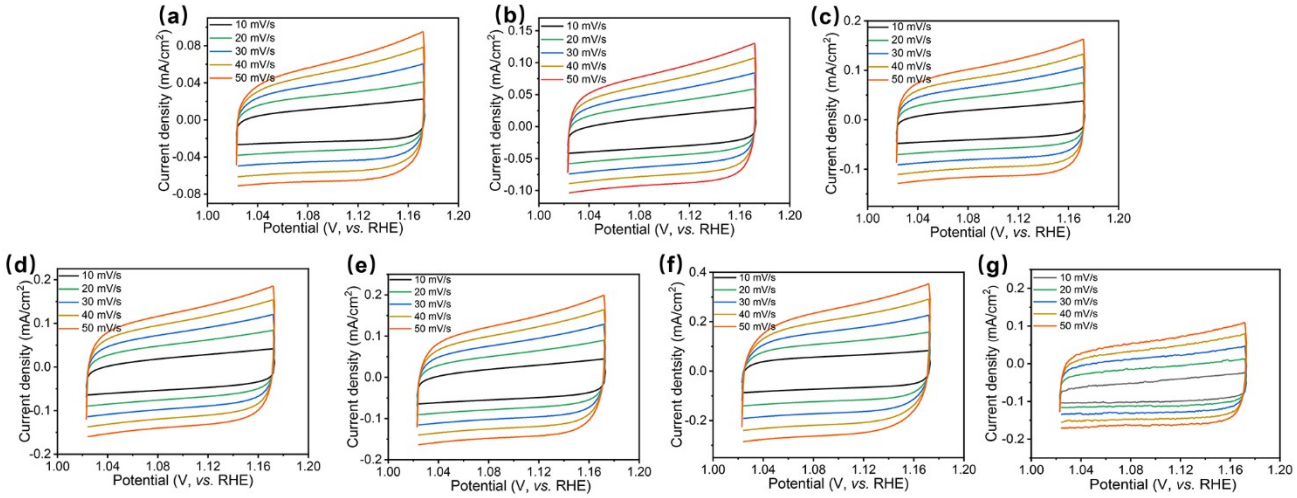

Figure S6 CV curves of (a) Ni foam, (b) NiFe LDH-NF, and F-NiFe LDH-NF electrodes with a treatment time of (c) 3 min, (d) 5 min, (e) 8 min, (f) 15 min, and (g) 30 min respectively at different scan rates from 10 to 50 mV/s.

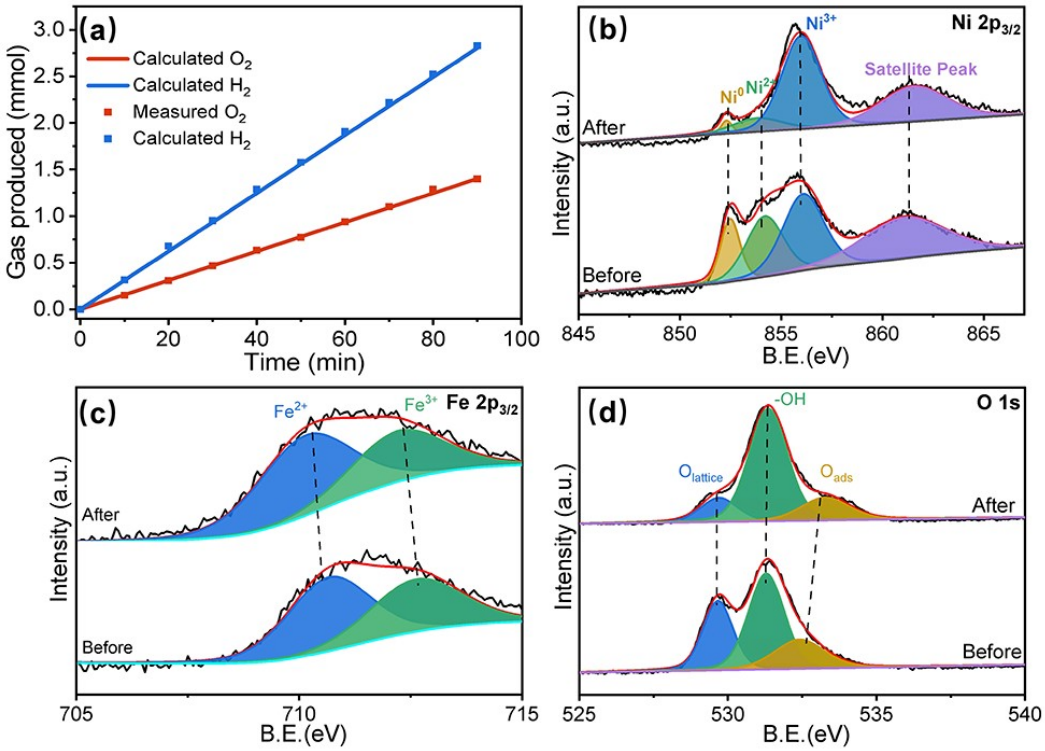

Figure S7 (a) The amount of gas products obtained from calculations and measurement in the saline electrolysis. High-resolution XPS of (b) Ni $2p_{3/2}$, (c) Fe $2p_{3/2}$, and (d) O 1s, respectively.

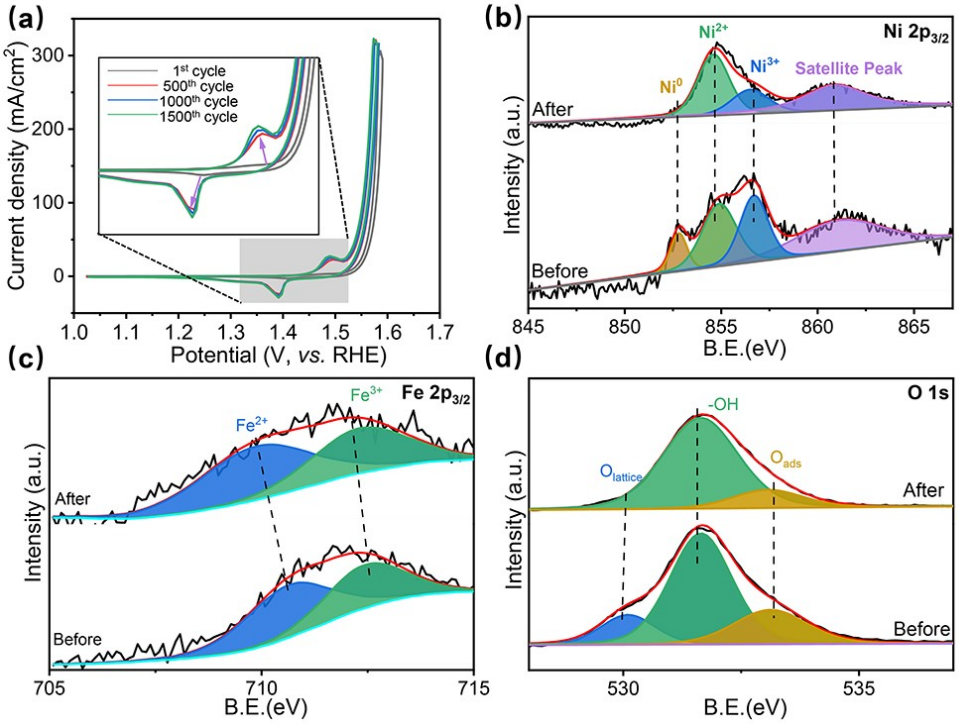

Figure S8 (a) Cyclic voltage curves of F-NiFe LDH-NF during 1500 cycles. The corresponding comparison in high-resolution XPS of (b) Ni $2p_{3/2}$, (c) Fe $2p_{3/2}$, and (d) O 1s, respectively before and after 1500 cycles.

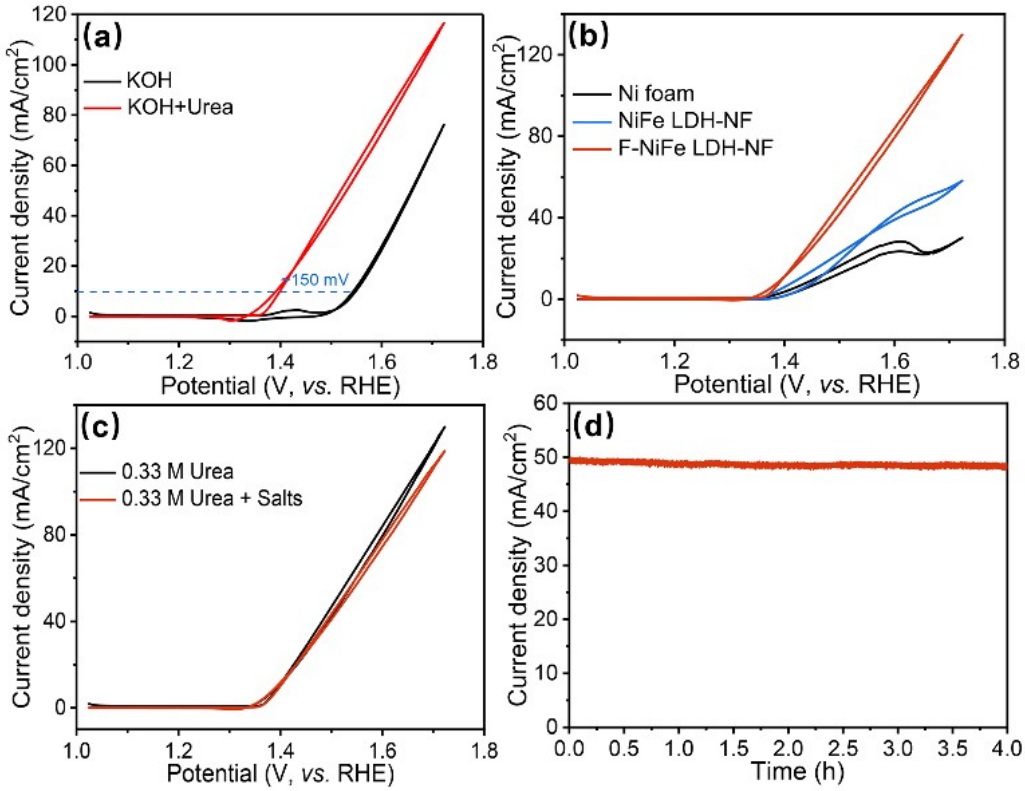

Figure S9 CV plots of (a) F-NiFe LDH-NF in 1 M KOH with/without 0.33 M urea, and (b) different electrodes in 1 M KOH with 0.33 M urea. (c) CV plots of F-NiFe LDH-NF in 1 M KOH and 0.33 M urea with/without other salts of urine, and (d) long-term electrolysis of F-NiFe LDH-NF in the simulated urine.

References:

1. W. Li, F. Li, H. Yang, X. Wu, P. Zhang, Y. Shan and L. Sun, *Nat. Commun.*, 2019, **10**, 1-11.
2. M. Khodabakhshi, S. Chen, T. Ye, H. Wu, L. Yang, W. Zhang and H. Chang, *ACS Appl. Mater. Interfaces*, 2020, **12**, 36268-36276.
3. B. You and Y. Sun, *Adv. Energy Mater.*, 2016, **6**, 1502333.
4. T. Zhao, C. Cheng, D. Wang, D. Zhong, G. Hao, G. Liu, J. Li and Q. Zhao, *ChemistrySelect*, 2021, **6**, 1320-1327.
5. B. Zhang, K. Jiang, H. Wang and S. Hu, *Nano Lett.*, 2018, **19**, 530-537.
6. S. Gao, Y. Lin, X. Jiao, Y. Sun, Q. Luo, W. Zhang, D. Li, J. Yang and Y. Xie, *Nature*, 2016, **529**, 68-71.
7. B. Zhou, C.-L. Dong, Y.-C. Huang, N. Zhang, Y. Wu, Y. Lu, X. Yue, Z. Xiao, Y. Zou and S. Wang, *J. Energy Chem.*, 2021, **61**, 179-185.
8. M. Gong, Y. Li, H. Wang, Y. Liang, J. Z. Wu, J. Zhou, J. Wang, T. Regier, F. Wei and H. Dai, *J. Am. Chem. Soc.*, 2013, **135**, 8452-8455.
9. J. Li, Y. Liu, H. Chen, Z. Zhang and X. Zou, *Adv. Funct. Mater.*, 2021, **31**, 2101820.
10. Z. Song, K. Wang, Q. Sun, L. Zhang, J. Li, D. Li, P. W. Sze, Y. Liang, X. Sun and X. Z. Fu, *Adv. Sci.*, 2021, **8**, 2100498.
11. W. Yuan, Z. Cui, S. Zhu, Z. Li, S. Wu and Y. Liang, *Electrochim. Acta*, 2021, **365**, 137366.
12. S. Gupta, M. Forster, A. Yadav, A. J. Cowan, N. Patel and M. Patel, *ACS Appl. Energy Mater.*, 2020, **3**, 7619-7628.
13. Y. Pan, Y. Yao, C. Liang, Y. Yang, J. Chen and Q. Li, *Mater. Lett.*, 2021, **302**, 130371.
14. T. Zhang, J. Du, P. Xi and C. Xu, *ACS Appl. Mater. Interfaces*, 2017, **9**, 362-370.
15. M. K. Sahoo, A. K. Samantara and J. Behera, *Inorg. Chem.*, 2020, **59**, 12252-12262.
16. N. R. Chodankar, I. V. Bagal, S. W. Ryu, Y. K. Han and D. H. Kim, *ChemCatChem*, 2019, **11**, 4256-4261.